THE JOURNAL OF PHYSICAL CHEMISTRY B
A JOURNAL OF THE AMERICAN CHEMICAL SOCIETY

pubs.acs.org/JPCB

Article

Direct Evidence for Excitation Energy Transfer Limitations Imposed by Low-Energy Chlorophylls in Photosystem I–Light Harvesting Complex I of Land Plants

Mattia Russo, Anna Paola Casazza, Giulio Cerullo, Stefano Santabarbara,* and Margherita Maiuri*

Cite This: *J. Phys. Chem. B* 2021, 125, 3566–3573

Read Online

ACCESS | Metrics & More | Article Recommendations | Supporting Information

ABSTRACT: The overall efficiency of photosynthetic energy conversion depends both on photochemical and excitation energy transfer processes from extended light-harvesting antenna networks. Understanding the trade-offs between increase in the antenna cross section and bandwidth and photochemical conversion efficiency is of central importance both from a biological perspective and for the design of biomimetic artificial photosynthetic complexes. Here, we employ two-dimensional electronic spectroscopy to spectrally resolve the excitation energy transfer dynamics and directly correlate them with the initial site of excitation in photosystem I–light harvesting complex I (PSI-LHCI) supercomplex of land plants, which has both a large antenna dimension and a wide optical bandwidth extending to energies lower than the peak of the reaction center chlorophylls. Upon preferential excitation of the low-energy chlorophylls (red forms), the average relaxation time in the bulk supercomplex increases by a factor of 2–3 with respect to unselective excitation at higher photon energies. This slowdown is interpreted in terms of an excitation energy transfer limitation from low-energy chlorophyll forms in the PSI-LHCI. These results aid in defining the optimum balance between the extension of the antenna bandwidth to the near-infrared region, which increases light-harvesting capacity, and high photoconversion quantum efficiency.

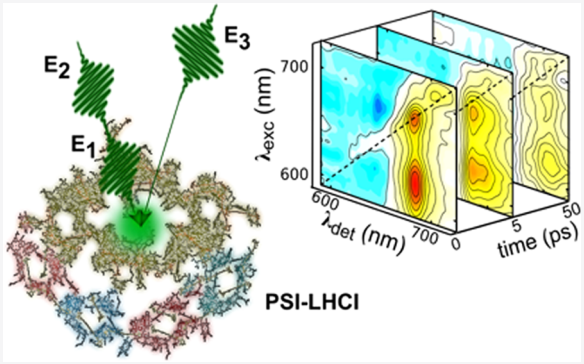

INTRODUCTION

Photosystem I (PSI) is one of the two pigment–protein supercomplexes essential for oxygenic photosynthesis, which mediate the light-driven electron transport from water to $NADP^+$. In land plants, PSI is organized into two functional and structural moieties: the core complex, harboring the reaction center (RC), where charge separation and successive electron transfer reactions occur, and an external antenna complex, collectively referred to as light harvesting complex I (LHCI). The PSI-LHCI supercomplex is considered as one of the best performing photochemical machineries known in nature, showing the highest efficiency among other photosystems, approaching unity.[1−3]

This very high photon conversion yield is maintained even though some light-harvesting antenna pigments absorb at lower energies than the RC chlorophylls (Chl), implying a thermodynamically unfavorable uphill excitation energy transfer (EET) to the photocatalytic site.[4] In higher plants, these low-energy absorbing chromophores, often referred to as "red forms", are mainly located in the LHCI antenna,[4−6] and are therefore, from a structural perspective, located at the periphery of the complex.[7] Moreover, more than one low-energy state is present in the LHCI, and each of the two dimers (Lhca1/Lhca4 and Lhca2/Lhca3) comprising it appears to bind a long-wavelength spectral form emitting at ∼730/735 nm.[8] This scenario is different from the case of cyanobacterial PSI, where the red forms, whose exact characteristics are species-dependent,[9] are instead located in the core complex, and hence spatially closer to the RC.

Since EET processes temporally overlap with the primary photochemical charge separation event and the first charge stabilization step, the direct and independent observation of these processes is challenging. The problem is further complicated by spectral congestion, since a large pigment–protein complex like PSI-LHCI binds, in total, over 150 Chls. As a result, the interpretation of the data often needs to rely on kinetic modeling. Thus, although both in the PSI of cyanobacteria[9−11] and in the PSI-LHCI supercomplex of higher plants[4,12,13] it has been proposed that uphill EET can limit the effective photochemical trapping time, the extent of this limitation remains to be unambiguously determined, at

Received: February 18, 2021
Published: March 31, 2021

least for the case of supercomplexes, in which the red forms are located in the external antenna.

From a biological perspective, the physiological role of red forms appears to be dominant under shading conditions, when photon fluxes are low and therefore the photosynthetic process is limited by light absorption and hence by the photon conversion efficiency.[14] It is moreover relevant to the understanding of photochemical processes in cyanobacteria that incorporate the intrinsically red-shifted Chl*f* in their antenna[15−17] and possibly also in the RC.[18] Furthermore, understanding the trade-off between the antenna bandwidth and the energy of the photocatalytic site can be of key importance for the design of broad-band artificial photosynthetic molecules and/or devices.

The most straightforward approach to test experimentally the limitations imposed by antenna red forms on EET and photochemical trapping processes is to perform experiments in which these forms are directly excited. Although some experimental evidences have been collected in cyanobacterial PSI, which consists of the core complex only, initially by time-resolved fluorescence[10,11] and successively by ultrafast transient absorption (TA)[19,20] and two-dimensional electronic spectroscopy (2DES),[21,22] limited direct information is available for the large PSI-LHCI supercomplex of higher plants.[23]

2DES is particularly powerful as it offers the possibility of directly test and cross-correlate the frequency of the initial site of excitation with the observed dynamics at a specific detection frequency on an ultrafast timescale. Recently, Akhtar et al.[23] studied both the core complex and the PSI-LHCI supercomplex of land plants using 2DES, but the excitation pulse bandwidth allowed only partial coverage of the long-wavelength absorption tail, up to ∼705 nm, therefore only partially covering the red forms absorption. Here, we investigate the excited-state dynamics in the PSI-LHCI supercomplex isolated from spinach by 2DES using ultra-broad-band pulses covering the 580−725 nm range, that allows us to explore direct red forms excitation in further detail. The complex was studied under both conditions of "open" and "closed" RCs (the latter achieved by chemical oxidation of the terminal electron donor P_{700}), thereby comparing EET in the presence and absence of photochemical quenching.

METHODS

Sample Preparation. PSI-LHCI was purified from unstacked spinach thylakoids as previously described.[13] The membranes were solubilized at 1 mg/mL Chl with 1% w/v *β*-dodecyl maltoside, which also replaced octylglucopyranoside in the successive sucrose density gradients. The PSI band from the sucrose gradient was concentrated by spinning at 180 000*g* for 2 h and finally resuspended in 25 mM tricine, 5 mM $MgCl_2$, and 0.003 w/v *β*-dodecyl maltoside. The sample at a concentration equivalent to 75 OD cm^{-1} was placed in a 200 *μ*m thick flow cuvette, and incubated with 30 mM sodium ascorbate and 150 *μ*M *N*,*N*,*N*′,*N*′-tetramethyl-*p*-phenylenediamine (TMPD) (open-center conditions) or 30 mM $K_3Fe(CN)_6$ (closed-center conditions).

Two-Dimensional Electronic Spectroscopy. 2DES simultaneously meets the requirements of high temporal and spectral resolution, exploiting the generation of the third-order nonlinear response function of the system after the interaction with three properly delayed broad-band laser pulses. Here, we adopted the partially collinear geometry in which the first two collinear phase-locked pulses delayed by a time t_1 (coherence time), generated by a birefringent interferometer, act as a pump. The third pulse acts as a probe and is delayed by the time t_2 (population or waiting time) with respect to the second pulse.[24] By acquiring the signal as a function of coherence time t_1 for a fixed population time t_2 and performing a Fourier transform with respect to t_1, one obtains two-dimensional excitation/detection correlation maps.

The ultra-broad-band visible pulses were generated by a noncollinear optical parametric amplifier in the visible and temporally compressed with a pair of chirped mirrors to reach sub-20-fs duration. The polarizations of the excitation and detection pulses were orthogonal to reduce the contribution of scattered light, which is almost unavoidable due to the dimension of the PSI-LHCI supercomplex. The adopted fluence was 28 *μ*J/cm^2, low enough to avoid singlet−singlet annihilation. The combination of high temporal resolution afforded by the broad-band laser pulses and high excitation/emission frequency resolution makes 2DES a perfect tool to study ultrafast processes in photosynthetic complexes. Experimental data were complemented by a global fitting procedure of the extended 2DES datasets.[25] Fitting of the early time dynamics, which requires considering the instrumental response function (IRF) of the system, was performed by convolving a multiexponential response with the IRF, given by the cross-correlation of the pump and probe pulses.

RESULTS AND DISCUSSION

Figure 1 shows four 2DES maps for PSI-LHCI under open-center conditions at waiting times t_2 = 75 fs, 1 ps, 10 ps, and 50 ps along with the steady-state absorption spectrum on the right and the excitation wavelength integrated 2DES spectra overlapped with the TA spectra on top. 2DES maps at t_2 = 75 fs and 1 ps show an intense diagonal peak at 680/680 nm excitation/detection wavelength, corresponding to the ground-state bleaching (GSB) of the Q_y transition of Chl*a* spectral forms responsible for the main absorption band (the so-called "bulk" Chls). The diagonal peak is accompanied by several off-

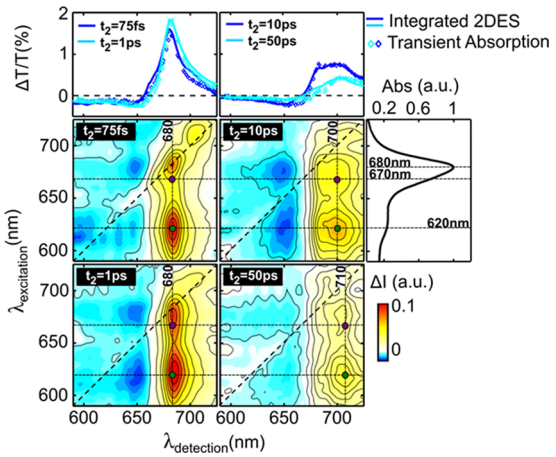

Figure 1. 2DES maps of the PSI-LHCI supercomplex under open-center conditions at four different waiting times: t_2 = 75 fs, 1 ps, 10 ps, and 50 ps. (Top) 2DES maps integrated along the excitation wavelength axis (solid lines) overlapped with the TA spectra (symbols). (Right) Portion of the steady-state absorption spectrum from 590 to 730 nm. Filled dots identify selected cross-peaks discussed in the text.

https://doi.org/10.1021/acs.jpcb.1c01498
J. Phys. Chem. B 2021, 125, 3566−3573

diagonal cross-peaks,[26] indicating both coupling and EET between the Q_y transition of bulk Chl*a* antenna chromophores and the shorter-wavelength Q_x band of Chl*a*, as well as both Q_y and Q_x bands of Chl*b*.

Intramolecular EET processes between the 0−0 (Q_y) transition and the coupled vibrational modes are however difficult to disentangle from intermolecular EET even by 2DES because of extensive spectral congestion, due to the large number of chromophores in the system, and because of inhomogeneous and homogeneous broadening of the transition energies. Yet it is worth noting that intramolecular EET, which is mediated by vibrational coupling, tends to localize the excitation on the diagonal of 2DES maps at early delays, whereas for excitation at wavelengths shorter than ∼675 nm, most of the intensity lies in the off-diagonal cross-peaks, indicating the occurrence of ultrafast EET from the short-wavelength spectral forms to the dominant absorption centered around 680 nm. The maps also present a broad and weak negative signal that corresponds to excited-state absorption (ESA) of the bulk Chls. The presence of ESA contributions might also mask the direct observation of vibronic coupling, as most of the partially resolved Chl vibronic progression falls in the same spectral window.

Moreover, a slight broadening of the main diagonal peak toward long wavelengths is detected already at t_2 = 75 fs and becomes more obvious at t_2 = 10 ps, when new cross-peaks centered around 700 nm are detected, close to the absorption peak of the electron donor P_{700}, which is an integral part of the RC. Further spectral evolution is observed at t_2 = 50 ps, when the position of the cross-peak shifts further to the red from 700 nm, i.e., into the spectral window dominated by Chl red forms.[4,12,27−29] This shift is mainly due to the relaxation of the residual GSB contribution from the bulk and moderately red-shifted Chl spectral forms, as the signal intensity in the long-wavelength tail is almost the same at t_2 = 10 and 50 ps (see the top right panel of Figure 1). Notably, at t_2 = 50 ps, the 2DES map still shows significant intensity at 700 nm, consistent with the photochemical population of the long-lived P_{700}^+ cation and demonstrating thereby the open state of the RCs in the complex. To gain further detail and decouple pure EET processes from the population of a long-lived radical pair following photochemical trapping, the 2DES experiments were also performed under closed-RC conditions, when P_{700} is preoxidized by ferricyanide. The corresponding maps are reported in Figure S2 in the Supporting Information (SI).

The 2DES maps acquired under both open- and closed-center conditions were decomposed by applying a global analysis algorithm to the data. This approach allows us to model the temporal evolution of the entire 2DES dataset with a series of exponential decays. The results of this analysis are expressed by two-dimensional decay associated spectra (2D-DAS) that are energy correlation maps showing the amplitude of a specific exponential decay for every point of the 2DES map.[25] The sign of the amplitude in the 2D-DAS allows one to identify formation or decay signals; specifically, a positive amplitude represents a positive exponential decay, meaning that GSB signals are decaying, and a negative amplitude identifies a negative exponential decay corresponding to GSB formation or ESA decay. Figure 2a reports the 2D-DAS for the PSI-LHCI supercomplex in open-RC conditions, corresponding to lifetimes of 0.3, 2.5, 12, 56, and >160 ps. The 2D-DAS of the PSI-LHCI supercomplex under closed-RC conditions are shown in Figure 2b and correspond to lifetimes of 0.2, 3.5, 22, and 78 ps. These values are in very good agreement with those previously reported for TA on the same sample[13] but recorded only for a limited number of pump wavelengths, all shorter than the RC resonance and with overall lower temporal resolution. Furthermore, they are rather close to the values observed in PSI-LHCI isolated from different plants[9,12,27−31] or from green algae[32−35] and compatible with the PSI core of cyanobacteria.[35−37]

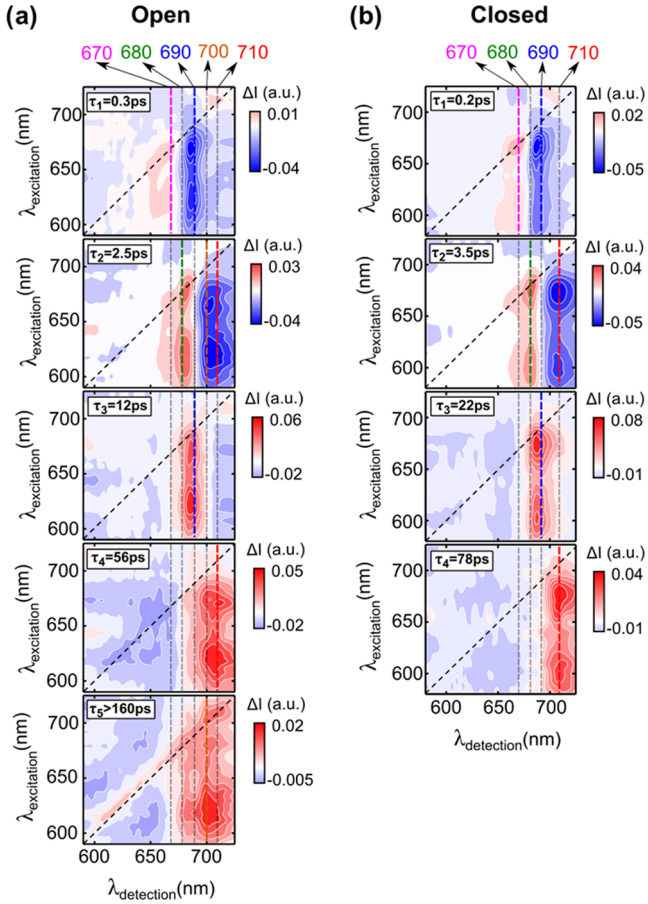

Figure 2. Global analysis results: (a) 2D-DAS maps of PSI-LHCI with open RCs. The temporal evolution of the system can be described with five time constants: 0.3, 2.5, 12, 56 ps, and a nondecaying component (limited by the maximum delay acquired for the measurement); (b) 2D-DAS maps of PSI-LHCI with closed RCs. Note the different colorbar scales for the open- and closed-RC configurations. The temporal evolution of the system can be described with four time constants: 0.2, 3.5, 22, and 78 ps. Slices of the 2D-DAS maps at representative wavelengths are presented in Figures S4 and S5 for open and closed centers, respectively.

The overall excited-state dynamics are not largely affected by the redox state of P_{700} (Figure 2b), in agreement with previous reports.[38−40] The additional long-lived component (>160 ps) under open-center conditions accounts for the contribution of P_{700}^+ whose decay is several orders of magnitude slower than the timescales of EET and primary electron transfer events. The longest-lived component under open-center conditions contains, however, also contributions from the red forms, as observable from the signal along the diagonal at wavelengths longer than 700 nm, which correspond to the ∼80 ps retrieved for closed-center conditions.

The 2D-DAS highlight the presence of two kinetic components of excited-state equilibration, one occurring on

https://doi.org/10.1021/acs.jpcb.1c01498
J. Phys. Chem. B 2021, 125, 3566−3573

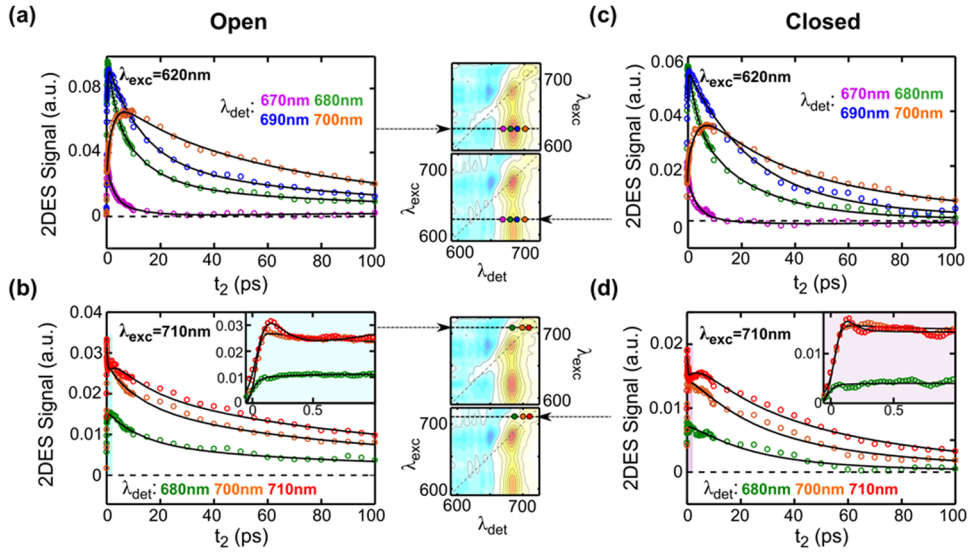

Figure 3. t_2 Time traces from the 2DES data of PSI-LHCI in (a) open- and (c) closed-center conditions obtained by exciting at 620 nm and probing at 670 nm (violet), 680 nm (green), 690 nm (blue), and 700 nm (orange). t_2 Time traces from the 2DES data of PSI-LHCI in (b) open and (d) closed configurations obtained by exciting at 710 nm (Chls red forms) and probing at 680 nm (green), 700 nm (orange), and 710 nm (red). In all panels, the dots represent the experimental data, and the continuous black lines are the fits obtained from the global analysis. The insets show a zoom on the kinetics up to 1 ps in which the best fit is obtained by convolution of the IRF of the system with multiexponential decays. For the open (closed) configuration, we used five (four) decays: τ_1−τ_5, where τ_3−τ_5 are fixed to the values obtained from the global analysis. The results are reported here. For λ_{probe} = 680 nm: τ_1 = 0.3 ps (0.3 ps), τ_2 = 2 ps (5 ps); for λ_{probe} = 700 nm: τ_1 = 0.35 ps (0.3 ps), τ_2 = 5 ps (3.5 ps); for λ_{probe} = 710 nm: τ_1 = 0.2 ps (0.4 ps), τ_2 = 5 ps (4 ps). The fits have an uncertainty of ±0.05 ps.

the subpicosecond timescale, and involving transfer to the bulk Chl forms, having a GSB maximum in correspondence to the 680 nm steady-state absorption peak, and a second phase, characterized by a lifetime of ca. 3−4 ps, corresponding to transfer to the low-energy forms, present both in the antenna and in the RC, considering that the absorption of P_{700} is in any case red-shifted with respect to the bulk of the antenna. The successive components are largely dominated by relaxation of the partially equilibrated state of the supercomplex, which is however faster for the bulk than for the long-wavelength states. Thus, from the inspection of the 2DES maps at selected delays and the 2D-DAS it is immediately appreciable that, when pumping at wavelengths shorter than ∼700 nm, the excited-state dynamics show very little dependence on the initial site of excitation. Interestingly, this also concerns preferential excitation of Chl*b* in the 630−650 nm window, where the relative contribution of this pigment is expected to be more relevant. For excitation at wavelengths shorter than the RC Chls absorption, the 0.3 ps component is dominated by EET to the bulk Chls; the 2.5−3.5 ps component contains contributions from slower equilibration with the low-energy antenna states, including those in the RC, as well as population of the primary radical pair;[12,23,31,34] the 10−20 ps component represents the main deexcitation of the bulk Chls, due to charge stabilization, and contains contributions also from the relaxation of a subpopulation of whole of red forms pools, whereas the slowly decaying component includes both the relaxation of the lowest-energy forms in the antenna and, under open-center conditions, also the signal due to the long-lived, stabilized, radical pair.

This general behavior, which accounts for excitation at wavelengths shorter than 700 nm, displays significant differences upon long-wavelength pumping. Despite the lifetimes being the same, the relative amplitudes, and therefore the overall excited-state dynamics, is distinct upon direct red forms excitation, as notable from the intensity and sign of the off-diagonal amplitudes in the 2D-DAS maps. A zoomed view of the 2D-DAS maps centered on the red-form absorption window is presented in Figure S3 of the SI.

This is also clearly illustrated in Figure 3 by the comparison of the kinetics (as a function of t_2) obtained by exciting the PSI-LHCI with open (Figure 3a,b) and closed RCs (Figure 3c,d). The kinetics at early times and the corresponding fits are reported in the insets of Figure 3b,d. Under open-RC conditions, upon unselective excitation at 620 nm (Figure 3a), mainly corresponding to the absorption peak of the Q_x band of Chl*a*, the kinetics monitored close to the absorption maximum (680 nm), after a very fast rise, decay promptly to the residual long-lived signal. This is due to both the nondecaying contribution of P_{700}^+ and to the slowest relaxation component from the red-most spectral forms. On the other hand, when the kinetics are monitored at 700 nm, which is a marker band for P_{700}^+ at open centers, a pronounced rise is observed, followed by a slow decay.

Upon excitation at 710 nm (Figure 3b), the observed dynamics change drastically. Even though at this wavelength the red forms are expected to be predominantly excited, partial excitation of the RC Chls is also expected because of the broad absorption bandwidth of P_{700}. The GSB signal of bulk Chls probed at 680 nm is characterized by a clear rise (a zoomed decay is highlighted in the inset of Figure 3b, green curve), indicating an uphill EET, whereas when monitoring either the RC Chls at 700 nm or the red forms at 710 nm (orange and red curves, respectively, in the inset of Figure 3b), a small but prompt decay to a nearly stationary level is observed. The fast relaxation (350 and 200 fs, respectively, for these two traces) can be interpreted as a contribution from EET of these moderately red-shifted forms to the more red-shifted states, as well as from the uphill EET to the bulk Chls.

https://doi.org/10.1021/acs.jpcb.1c01498
J. Phys. Chem. B 2021, 125, 3566−3573

The difference in the overall dynamics, depending on the site of excitation, can be compactly visualized by contour plots of the first moment of the decay distribution, τ_m (defined as $\tau_m(\lambda_1,\lambda_2) = \sum_i A_i(\lambda_1,\lambda_2)\cdot\tau_i^2/\sum_i A_i(\lambda_1,\lambda_2)\cdot\tau_i$, where $A_i(\lambda_1,\lambda_2)$ are the 2D-DAS and τ_i are the corresponding lifetimes; see also Section IV of the SI for further details). The application of decay moments is common practice in the analysis of time-resolved fluorescence data.[39] However, despite the generality of the approach, it has been seldom applied to TA experiments, and it is here nonetheless extended to the analysis of 2DES data. Figure 4 shows the τ_m contour map (Figure 4a) together

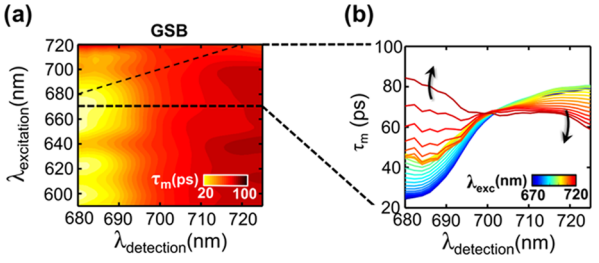

Figure 4. (a) τ_m Map derived from the 2D-DAS of Figure 2b for PSI-LHCI under closed-center conditions, in the GSB-dominated spectral window. (b) Slices showing the wavelength dependence of τ_m at selected pump wavelengths.

with slices at selected excitation wavelengths, calculated for closed-center conditions for pump wavelengths >670 nm (Figure 4b). For open centers, the estimation of τ_m is made more cumbersome by the presence of the nondecaying P_{700}^+ contribution, which needs to be fully deconvoluted to avoid distortions in the parameter estimation. Nonetheless, due to the observed similarity of the relaxation for open and closed centers, we consider the information obtained from the latter as significant also for fully photochemically active conditions. The observed rapid excited-state decay at closed centers is due to either a direct quenching by P_{700}^+ or, more likely, to nonradiative deexcitation to the ground state of a photochemically populated radical pair which cannot be further stabilized when P_{700} is already oxidized.[40,41] Therefore, it can be considered as a "pseudo-photochemical" quenching process. In both cases, any EET migration limitation from the antenna to RC would remain even at closed centers.

The contour map of τ_m for the GSB-dominated region (Figure 4a) shows that, for excitation at wavelengths shorter than 700 nm, the first moment of the decay kinetics increases smoothly from short to long detection wavelengths. This is in analogy to what observed previously in fluorescence lifetime studies but calculating the average lifetimes, τ_{av}, defined as $\tau_{av}(\lambda_1) = \sum_i A_i(\lambda_1)\cdot\tau_i/\sum_i A_i(\lambda_1)$, that corresponds to an amplitude-weighted zero-order moment of the decay distribution[4,28,29,42] (see also the SI for a brief discussion). The smooth increase of τ_m toward long wavelengths can be interpreted in terms of a partial energy diffusion barrier associated with equilibration on the antenna red forms. This behavior appears slightly more pronounced for excitation in the 630−645 nm window, which is where Chl*b* (Q_y) absorbs predominantly (see Figure S6 in the SI). Since Chl*b* is bound to the LHCI complexes that also harbor the red forms, the slightly more pronounced increase in τ_m is interpretable in terms of slower energy equilibration between the external antenna complexes, due to preferential coupling with the low-energy Chls, rather than in terms of slow EET from Chl*b* spectral forms themselves. On the other hand, the trend observed is remarkably different upon direct excitation of the red forms at wavelengths longer than 700 nm. Their direct relaxation becomes somewhat faster because of the prompt depopulation of these states associated with uphill EET to shorter-wavelength-absorbing pigments. Most significantly, the value of τ_m for the bulk Chls increases considerably when exciting above ∼700 nm. The progressive slowdown of the excited-state dynamics upon excitation at longer wavelengths is evidenced by the selected slices of the contour map reported in Figure 4b.

The direct correlation between excitation and detection wavelength provided by 2DES demonstrates unambiguously the impact of low-energy Chls red forms on the overall deexcitation dynamics in PSI. Our analysis performed on systems with closed centers can be reasonably extended to the open-center case. The slowing down of the dynamics upon excitation of the red forms is sizable for the bulk Chls, with a progressive lengthening of the mean decay lifetime from a factor of ≈2, when exciting at 700 nm, to a factor of ≈3 in the 705−715 nm pump wavelength window. Nevertheless, the dynamics remain relatively rapid, as the highest value of τ_m is ≈80−90 ps, which is over 20 times faster than the natural lifetime of Chls in the absence of photochemical and/or dissipative processes (∼2 ns). Thus, although the presence of antenna states red-shifted by 20−30 nm with respect to the RC Chls negatively affects the EET dynamics and, consequently, the overall trapping dynamics, the photon utilization efficiency remains close to unity.

CONCLUSIONS

PSI is an intriguing system from the photochemical perspective, because it operates with an extremely high photon conversion quantum efficiency, approaching unity, even in the presence of energy states in its antenna network that absorb at lower energy than the chromophore involved in photochemical conversion. Thermodynamic reasoning would imply a competition for localization of the excited states between the RC and the low-energy Chl red forms, which should then decrease the photon conversion quantum efficiency. Although limitations imposed by EET have been previously observed by employing 2DES for the cyanobacterial core system, which has an antenna network dimension of ∼80 Chl/RC,[9−11,19,20] we have here demonstrated a significant effect of low-energy Chls on the overall trapping/EET dynamics even in the larger (∼150 Chl) RC of higher plants, where the red forms are located much further at the periphery of the supercomplex. The extent of EET slowing down correlates with the specific energy of the red form, being more pronounced for the red-most forms, which have been attributed to Chls bound to the Lhca3 and Lhca4 complexes.[6,8,43−45] At the same time, EET from the high-energy absorbing chromophore Chl*b*, which is also bound to LHCI, and that can be simultaneously investigated by broad-band 2DES, is less pronounced. This seems to indicate that the slower EET is not due to slow Chl*b* to Chl*a* EET, but rather to the co-localization of Chl*b* and the red forms in the LHCI complexes.

These results allow us to conclude that it is the energy level of the chromophores, rather than their specific location within the photosystem with respect to the RC, which contributes the most to their energetic equilibration dynamics. This is a relevant piece of information for defining within a general framework the balance between increase of antenna bandwidth

https://doi.org/10.1021/acs.jpcb.1c01498
J. Phys. Chem. B 2021, 125, 3566−3573

and optimization of quantum conversion efficiency in complex chromophore networks comprising molecules absorbing at longer wavelengths than the site of photochemical energy conversion. Our conclusions are relevant both to biology, where red forms are widespread but strongly organism-dependent,[46] and to the *de novo* design of artificial light-harvesting materials.

■ ASSOCIATED CONTENT

Supporting Information

The Supporting Information is available free of charge at https://pubs.acs.org/doi/10.1021/acs.jpcb.1c01498.

Section I: general structure of the PSI-LHCI supercomplex and superimposition of the laser bandwidth used in 2DES measurements on the steady-state absorption spectrum; Section II: 2DES maps for PSI-LHCI at closed-center conditions; Section III: expanded 2DES maps at representative t_2 delays and 2D-DAS focused on the red-form-dominated spectral window. Also shown in this section are the DAS at selected pump wavelengths, sliced from the 2D-DAS maps of Figure 3 to allow direct comparison with classic TA measurements; Section IV: comparison of τ_m slices across the pump axis (from Figure 4) with TC-SPC results from previous studies; Section V: reproducibility of the results and analysis; and an independent dataset, acquired under similar experimental conditions is presented to support the reproducibility of all of the main spectra and kinetic features reported in the main text (PDF)

■ AUTHOR INFORMATION

Corresponding Authors

Stefano Santabarbara − *Photosynthesis Research Unit, Centro Studi sulla Biologia Cellulare e Molecolare delle Piante, Consiglio Nazionale delle Ricerche, 20133 Milano, Italy;* orcid.org/0000-0002-7993-2614; Phone: +39 02 503 14857; Email: stefano.santabarbara@cnr.it

Margherita Maiuri − *Istituto di Fotonica e Nanotecnologie del Consiglio Nazionale delle Ricerche, Dipartimento di Fisica, Politecnico di Milano, 20133 Milano, Italy;* orcid.org/0000-0001-9351-8551; Email: margherita.maiuri@polimi.it

Authors

Mattia Russo − *Istituto di Fotonica e Nanotecnologie del Consiglio Nazionale delle Ricerche, Dipartimento di Fisica, Politecnico di Milano, 20133 Milano, Italy*

Anna Paola Casazza − *Istituto di Biologia e Biotecnologia Agraria, Consiglio Nazionale delle Ricerche, 20133 Milano, Italy;* orcid.org/0000-0001-6129-3722

Giulio Cerullo − *Istituto di Fotonica e Nanotecnologie del Consiglio Nazionale delle Ricerche, Dipartimento di Fisica, Politecnico di Milano, 20133 Milano, Italy;* orcid.org/0000-0002-9534-2702

Complete contact information is available at: https://pubs.acs.org/10.1021/acs.jpcb.1c01498

Author Contributions

M.R., S.S., and M.M. performed measurements and analyzed the results. S.S. and A.P.C. purified the supercomplex and performed preliminary analysis. S.S., G.C., M.M., and A.P.C. designed the research. M.M., M.R., S.S., and G.C. wrote the manuscript. The manuscript was written through contributions of all authors. All authors have given approval to the final version of the manuscript.

Notes

The authors declare no competing financial interest.

■ ACKNOWLEDGMENTS

S.S. and A.P.C. acknowledge support for this research from Fondazione Cariplo (CYAO project, grant number 2016-0667) and thank Dr. A. Petrova for the assistance in biochemical sample preparation. G.C. acknowledges the support from the PRIN 2017 Project 201795SBA3−HARVEST. The authors thank Dr. A. Volpato and Prof. E. Collini for sharing the software for the global analysis of 2DES maps.

■ ABBREVIATIONS

PSI-LHCI, photosystem I−light harvesting complex I; RC, reaction center; EET, excitation energy transfer; Chl, chlorophyll; TA, transient absorption; 2DES, two-dimensional electronic spectroscopy; TMPD, tetramethyl-*p*-phenylenediamine; GSB, ground-state bleaching; ESA, excited-state absorption; 2D-DAS, 2D-decay associated spectra

■ REFERENCES

(1) Croce, R.; van Amerongen, H. Light-harvesting in Photosystem I. *Photosynth. Res.* **2013**, *116*, 153−166.

(2) Caffarri, S.; Tibiletti, T.; Jennings, R. C.; Santabarbara, S. A Comparison between Plant Photosystem I and Photosystem II Architecture and Functioning. *Curr. Protein Pept. Sci.* **2014**, *15*, 296−331.

(3) Nelson, N.; Junge, W. Structure and energy transfer in photosystems of oxygenic photosynthesis. *Annu. Rev. Biochem.* **2015**, *84*, 659−683.

(4) Jennings, R. C.; Zucchelli, G.; Croce, R.; Garlaschi, F. M. The photochemical trapping rate from red spectral states in PSI−LHCI is determined by thermal activation of energy transfer to bulk chlorophylls. *Biochim. Biophys. Acta* **2003**, *1557*, 91−98.

(5) Croce, R.; Zucchelli, G.; Garlaschi, F. M.; Bassi, R.; Jennings, R. C. Excited state equilibration in the Photosystem I-Light-Harvesting I Complex: P700 is almost isoenergetic with its antenna. *Biochemistry* **1996**, *35*, 8572−8579.

(6) Croce, R.; Zucchelli, G.; Garlaschi, F. M.; Jennings, R. C. A thermal broadening study of the antenna chlorophylls in PSI-200, LHCI, and PSI Core. *Biochemistry* **1998**, *37*, 17355−17360.

(7) Mazor, Y.; Borovikova, A.; Nelson, N. The structure of plant photosystem I super-complex at 2.8 Å resolution. *eLife* **2015**, *4*, No. e7433.

(8) Wientjes, E.; Croce, R. The light-harvesting complexes of higher-plant Photosystem I: Lhca1/4 and Lhca2/3 form two red-emitting heterodimers. *Biochem. J.* **2011**, *433*, 477−485.

(9) Gobets, B.; van Grondelle, R. Energy transfer and trapping in Photosystem I. *Biochim. Biophys. Acta* **2001**, *1507*, 80−99.

(10) Gobets, B.; van Stokkum, I. H.; Rögner, M.; Kruip, J.; Schlodder, E.; Karapetyan, N. V.; Dek-ker, J. P.; van Grondelle, R. Time-resolved fluorescence emission measurements of Photosystem I particles of various cyanobacteria: a unified compartmental model. *Biophys. J.* **2001**, *81*, 407−424.

(11) Gobets, B.; Valkunas, L.; van Grondelle, R. Bridging the gap between structural and lattice models: A parameterization of energy transfer and trapping in Photosystem I. *Biophys. J.* **2003**, *85*, 3872−3882.

(12) Wientjes, E.; Van Stokkum, I. H.; Van Amerongen, H.; Croce, R. Excitation energy transfer dynamics of higher plant photosystem I light harvesting complexes. *Biophys. J.* **2011**, *100*, 1372−1380.

(13) Molotokaite, E.; Remelli, W.; Casazza, A. P.; Zucchelli, G.; Polli, D.; Cerullo, G.; Santabarbara, S. Trapping dynamics in Photosystem I-Light Harvesting Complex I of higher plants is governed by the competition between excited state diffusion from low energy states and photochemical charge separation. *J. Phys. Chem. B* **2017**, *121*, 9816−9830.
(14) Rivadossi, A.; Zucchelli, G.; Garlaschi, F. M.; Jennings, R. C. The importance of PS I chlorophyll red forms in light-harvesting by leaves. *Photosynth. Res.* **1999**, *60*, 209−215.
(15) Gan, F.; Shen, G.; Bryant, D. A. Occurrence of Far-Red light photoacclimation (FaRLiP) in diverse cyanobacteria. *Life* **2015**, *5*, 4−24.
(16) Kurashov, V.; Ho, M. Y.; Shen, G.; Piedl, K.; Laremore, T. N.; Bryant, D. A.; Golbeck, J. H. Energy transfer from chlorophyll f to the trapping center in naturally occurring and engineered Photosystem I complexes. *Photosynth. Res.* **2019**, *141*, 151−163.
(17) Cherepanov, D. A.; Shelaev, I. V.; Gostev, F. E.; Aybush, A. V.; Mamedov, M. D.; Shen, G.; Nadtochenko, V. A.; Bryant, D. A.; Semenov, A.Yu.; Golbeck, J. H. Evidence that chlorophyll *f* functions solely as an antenna pigment in far-red-light photosystem I from *Fischerellathermalis* PCC 7521. *Biochim. Biophys. Acta* **2020**, *1861*, No. 148184.
(18) Nürnberg, D. J.; Morton, J.; Santabarbara, S.; Telfer, A.; Joliot, P.; Antonaru, L. A.; Ruban, A. V.; Cardona, T.; Krausz, E.; Boussac, A.; Fantuzzi, A.; Rutherford, A. W. Photochemistry beyond the red limit in chlorophyll *f*-containing photosystems. *Science* **2018**, *360*, 1210−1213.
(19) Cherepanov, D. A.; Shelaev, I. V.; Gostev, F. E.; Mamedov, M. D.; Petrova, A. A.; Aybush, A. V.; Shuvalov, V. A.; Semenov, A. Y.; Nadtochenko, V. A. Mechanism of adiabatic primary electron transfer in photosystem I: Femtosecond spectroscopy upon excitation of reaction center in the far-red edge of the Q_Y band. *Biochim. Biophys. Acta* **2017**, *1858*, 895−905.
(20) Cherepanov, D. A.; Shelaev, I. V.; Gostev, F. E.; Mamedov, M. D.; Petrova, A. A.; Aybush, A. V.; Shuvalov, V. A.; Semenov, A. Y.; Nadtochenko, V. A. Excitation of photosystem I by 760 nm femtosecond laser pulses: transient absorption spectra and intermediates. *J. Phys. B: At. Mol. Phys.* **2017**, *50*, No. 174001.
(21) Anna, J. M.; Ostroumov, E. E.; Maghlaoui, K.; Barber, J.; Scholes, G. D. Two-Dimensional Electronic spectroscopy reveals ultrafast downhill energy transfer in Photosystem I trimers of the cyanobacterium *Thermosynechococcus elongatus*. *J. Phys. Chem. Lett.* **2012**, *3*, 3677−3684.
(22) Lee, Y.; Gorka, M.; Golbeck, J. H.; Anna, J. M. Ultrafast energy transfer involving the red chlorophylls of cyanobacterial Photosystem I probed through Two-Dimensional Electronic Spectroscopy. *J. Am. Chem. Soc.* **2018**, *140*, 11631−11638.
(23) Akhtar, P.; Zhang, C.; Liu, Z.; Tan, H. S.; Lambrev, P. H. Excitation transfer and trapping kinetics in plant Photosystem I probed by two-dimensional electronic spectroscopy. *Photosynth. Res.* **2018**, *135*, 239−250.
(24) Réhault, J.; Maiuri, M.; Oriana, A.; Cerullo, G. Two-dimensional electronic spectroscopy with birefringent wedges. *Rev. Sci. Instrum.* **2014**, *85*, No. 123107.
(25) Volpato, A.; Bolzonello, L.; Meneghin, E.; Collini, E. Global analysis of coherence and population dynamics in 2D electronic spectroscopy. *Opt. Express* **2016**, *24*, 24773−24785.
(26) Cho, M.; Vaswani, H. M.; Brixner, T.; Stenger, J.; Fleming, G. R. Exciton analysis in 2D electronic spectroscopy. *J. Phys. Chem. B* **2005**, *109*, 10542−10556.
(27) Croce, R.; Dorra, D.; Holzwarth, A. R.; Jennings, R. C. Fluorescence decay and spectral evolution in intact photosystem I of higher plants. *Biochemistry* **2000**, *39*, 6341−6348.
(28) Engelmann, E.; Zucchelli, G.; Casazza, A. P.; Brogioli, D.; Garlaschi, F. M.; Jennings, R. C. Influence of the photosystem I-light harvesting complex I antenna domains on fluorescence decay. *Biochemistry* **2006**, *45*, 6947−6955.
(29) Jennings, R. C.; Zucchelli, G.; Santabarbara, S. Photochemical trapping heterogeneity as a function of wavelength, in plant photosystem I (PSI-LHCI). *Biochim. Biophys. Acta* **2013**, *1827*, 779−785.
(30) Kumazaki, S.; Ikegami, I.; Furusawa, H.; Yasuda, S.; Yoshihara, K. Observation of the excit-ed state of the primary electron donor chlorophyll (P700) and the ultrafast charge separation in the spinach Photosystem I reaction center. *J. Phys. Chem. B* **2001**, *105*, 1093−1099.
(31) Slavov, C.; Ballottari, M.; Morosinotto, T.; Bassi, R.; Holzwarth, A. R. Trap-limited charge separation kinetics in higher plant photosystem I complexes. *Biophys. J.* **2008**, *94*, 3601−3612.
(32) Melkozernov, A. N.; Kargul, J.; Lin, S.; Barber, J.; Blankenship, R. E. Energy coupling in the PSI-LHCI Supercomplex from the green alga *Chlamydomonas reinhardtii*. *J. Phys. Chem. B* **2004**, *108*, 10547−10555.
(33) Gibasiewicz, K.; Ramesh, V. M.; Melkozernov, A. N.; Lin, S.; Woodbury, N. W.; Blankenship, R. E.; Webber, A. N. Excitation dynamics in the core antenna of PS I from *Chlamydomonas reinhardtii* CC 2696 at room temperature. *J. Phys. Chem. B* **2001**, *105*, 11498−11506.
(34) Müller, M. G.; Niklas, J.; Lubitz, W.; Holzwarth, A. R. Ultrafast transient absorption studies on Photosystem I reaction centers from *Chlamydomonas reinhardtii*. 1. A new interpretation of the energy trapping and early electron transfer steps in Photosystem I. *Biophys. J.* **2003**, *85*, 3899−3922.
(35) Savikhin, S.; Xu, W.; Chitnis, P. R.; Struve, W. S. Ultrafast primary processes in PS I from *Synechocystis sp*. PCC 6803: roles of P700 and A0. *Biophys. J.* **2000**, *79*, 1573−1586.
(36) Shelaev, I. V.; Gostev, F. E.; Mamedov, M. D.; Sarkisov, O. M.; Nadtochenko, V. A.; Shuvalov, V. A.; Semenov, A. Y. Femtosecond primary charge separation in *Synechocystis sp*. PCC 6803 photosystem I. *Biochim. Biophys. Acta* **2010**, *1797*, 1410−1420.
(37) Cherepanov, D. A.; Shelaev, I. V.; Gostev, F. E.; Aybush, A. V.; Mamedov, M. D.; Shuvalov, V. A.; Semenov, A. Y.; Nadtochenko, V. A. Generation of ion-radical chlorophyll states in the light-harvesting antenna and the reaction center of cyanobacterial photosystem I. *Photosynth. Res.* **2020**, *146*, 55−73.
(38) Byrdin, M.; Rimke, I.; Schlodder, E.; Stehlik, D.; Roelofs, T. A. Decay kinetics and quantum yields of fluorescence in Photosystem I from *Synechococcus elongatus* with P700 in the reduced and oxidized state: are the kinetics of excited state decay trap-limited or transfer-limited? *Biophys. J.* **2000**, *79*, 992−1000.
(39) Lakowicz, J. R. *Principles in Fluorescence Spectroscopy*; Plenum Press: New York, 1983.
(40) Giera, W.; Ramesh, V. M.; Webber, A. N.; van Stokkum, I. H. M.; van Grondelle, R.; Giba-siewicz, K. Effect of the P700 pre-oxidation and point mutations near A0 on the reversibility of the primary charge separation in Photosystem I from *Chlamydomonas reinhardtii*. *Biochim. Biophys. Acta* **2010**, *1797*, 106−112.
(41) Russo, M.; Petropoulos, V.; Molotokaite, E.; Cerullo, G.; Casazza, A. P.; Maiuri, M.; Santabarbara, S. Ultrafast excited state dynamics in land plants Photosystem I core and whole super-complex under oxidised electron donor conditions. *Photosynth. Res.* **2020**, *144*, 221−233.
(42) Santabarbara, S.; Tibiletti, T.; Remelli, W.; Caffarri, S. Kinetics and heterogeneity of energy transfer from Light Harvesting Complex II to Photosystem I in the supercomplex isolated from arabidopsis. *Phys. Chem. Chem. Phys.* **2017**, *19*, 9210−9222.
(43) Morosinotto, T.; Mozzo, M.; Bassi, R.; Croce, R. Pigment-pigment interactions in Lhca4 antenna complex of higher plants photosystem I. *J. Biol. Chem.* **2005**, *280*, 20612−20619.
(44) Mozzo, M.; Morosinotto, T.; Bassi, R.; Croce, R. Probing the structure of Lhca3 by mutation analysis. *Biochim. Biophys. Acta* **2006**, *1757*, 1607−1613.
(45) Jennings, R. C.; Zucchelli, G.; Engelmann, E.; Garlaschi, F. M. The long-wavelength chlorophyll states of plant LHCI at room temperature: a comparison with PSI-LHCI. *Biophys. J.* **2004**, *87*, 488−497.
(46) Santabarbara, S.; Casazza, A. P.; Belgio, E.; Kaňa, R.; Prášil, O. Light Harvesting by Long-Wavelength Chlorophyll Forms (Red

https://doi.org/10.1021/acs.jpcb.1c01498
J. Phys. Chem. B 2021, 125, 3566−3573

Forms) in Algae: Focus on their Presence, Distribution and Function in Photosynthesis. In *Algae: Biochemical and Physiological Mechanisms*; Larkum, A. D.; Grossmann, A. R.; Raven, J. A., Eds.; Springer Nature: Switzerland, 2020; pp 261−297.

https://doi.org/10.1021/acs.jpcb.1c01498
J. Phys. Chem. B 2021, 125, 3566−3573